



ACADEMIC
PRESS

Available online at www.sciencedirect.com

SCIENCE @ DIRECT®

Icarus 161 (2003) 181–191

ICARUS

www.elsevier.com/locate/icarus

Resolution of the Kuiper belt object color controversy: two distinct color populations

S.C. Tegler^{a,*} and W. Romanishin^{b,1}

^a Department of Physics and Astronomy, Northern Arizona University Flagstaff, AZ 86011, USA

^b Department of Physics and Astronomy, University of Oklahoma, Norman, OK 73019, USA

Received 1 March 2002; revised 10 June 2002

Abstract

Four years ago, we reported that the surface colors of ancient, icy bodies at and beyond the orbit of Neptune—Kuiper belt objects—divide into two distinct color populations. Our report has proven quite controversial. Specifically, every other research group looking with large telescopes at Kuiper belt objects finds a continuous range of colors rather than two distinct populations. Here we report new color measurements of 18 objects, primarily from the Keck I 10-m telescope, that confirm the existence of two populations. We have combined the color measurements of the other groups to create a data set comparable in size to our data set. We have carried out a Monte Carlo statistical analysis and found that both data sets are consistent with two color populations and our data set, which has smaller uncertainties, rules out a continuum of colors. In addition, our new observations and those in the literature confirm our earlier report that classical KBOs with perihelion distances beyond 40 AU exhibit extremely red surface colors. Our results rule out a continuous color distribution for both our complete sample and subsamples with perihelion distances greater than or less than 40 AU. We suspect the color patterns will result in a better understanding of the formation and evolution of the outer Solar System.

© 2003 Elsevier Science (USA). All rights reserved.

Keywords: Centaurs; Kuiper belt objects; Trans-Neptunian objects

I. Introduction

Optical photometry is a powerful tool in the study of Kuiper belt objects (KBOs) because it is currently the only technique that we can use to observe a significant fraction of the ~500 known KBOs using a practical amount of observing resources. Accurate photometric observations of very large numbers of KBOs make it possible to look for correlations between their surface colors and dynamical properties. The discovery of such correlations are likely to result in a better understanding of the formation and evolution of the outer Solar System.

During the last four years, a controversy has arisen con-

cerning the optical colors of KBOs. In 1996, Luu and Jewitt reported that 15 KBOs and Centaurs (recent escapees from the Kuiper belt on outer-planet-crossing orbits) exhibit a continuum of colors ranging from solar to some of the reddest objects in the Solar System. Luu and Jewitt devised a mechanism consisting of steady radiation reddening and stochastic impact graying to explain the continuum of colors. In their mechanism, occasional impacts by smaller KBOs excavate pristine, gray, icy material from beneath the red crusts of larger KBOs. Their mechanism predicts an azimuthal color variation on individual KBOs equal to the color range among objects. In 1998, Jewitt and Luu published colors for four more objects.

In 1998 we reported a surprising result—the colors of 16 KBOs and Centaurs divide into two distinct groups, solar and extremely red (Tegler and Romanishin, 1998). In 2000, we reported colors for 21 more objects and confirmed the existence of two distinct groups (Tegler and Romanishin, 2000). In addition, we reported the first correlation between

* Corresponding author. Fax: +1-928-523-1371.

E-mail addresses: Stephen.Tegler@nau.edu (S.C. Tegler); wjr@nhn.ou.edu (W. Romanishin).

¹ Observers at the Keck I, Bok, and Vatican Advanced Technology telescopes.

surface colors of KBOs and a dynamical property—KBOs on near-circular orbits beyond 40 exhibit only extremely red surface colors.

In 2001, Jewitt and Luu reported colors of 17 more KBOs and Centaurs and remeasurements of eight objects from their previous two papers. In their analysis, they point out that our measurements and their measurements are in agreement and our difference resides in the interpretation of the data. They carry out a statistical analysis using the binomial probability distribution and find there is a 13% probability that a continuum of colors will result in the distribution we see and that we incorrectly describe as two groups. Strictly speaking, their analysis says our assertion of two color populations is a weak result. Jewitt and Luu never assume two populations in their statistical analysis, so they cannot rule out two color populations. Furthermore, we disagree with their entire statistical analysis and the 13% probability because they do not take into account that uncertainties in color measurements are capable blurring two color populations into a continuum of colors.

Until a few months ago, there may have been a tendency for an impartial observer of the controversy to sway more toward a continuum of colors than toward two groups because Luu and Jewitt (1996) put forth a physical mechanism to explain a continuum of colors. We point out that Jewitt and Luu (2001) admit there is a serious blow against their radiation reddening and collisional graying mechanism—repeated measurements of KBOs taken at random rotational phases are in general agreement within the uncertainties, while color differences among KBOs are many times larger than the measurement uncertainties. Jewitt and Luu admit “the primary origin of the color dispersion remains unknown.” At present, there is no mechanism that explains either a continuum of colors or two color populations.

In the discussion below, we examine two large samples of objects—our sample (Tegler and Romanishin, 1998; Tegler and Romanishin, 2000; and new measurements reported here for the first time) and a comparison sample from the literature also observed with very large telescopes (Barucci et al., 1999; Barucci et al., 2000; Boehnhardt et al., 2001; Delsanti et al., 2001; Jewitt and Luu, 2001; Doresoundiram et al., 2002)—for the signatures of two color populations and a continuum of colors.

II. Observations

The majority of the colors we report here come from the Low-Resolution Imaging Spectrometer (LRIS), B(438 nm), V (547 nm), and R (642 nm) glass filters, and a dichroic element (D460) that allows us to simultaneously observe with two (2,048 × 2,048)-pixel charge coupled device (CCD) cameras at the f/15 Cassegrain focus of the 10-m Keck I telescope (Oke et al., 1995). Each of our images covers 6 × 7 arcmin on the sky at 0.21 arcsec pixel⁻¹ and has a median stellar point-spread function full-width at

half-maximum of about 0.7 arcsec. Here we describe our latest observations during three photometric nights, 2001 May 21–23 UT, as well as our data reduction and analysis procedures.

We use the Image Reduction and Analysis Facility (IRAF) for CCD reduction and analysis tasks. After bias subtraction and flatfielding, we examine each KBO image for contamination by cosmic rays, faint background stars, and faint background galaxies. We discard any KBO images with contamination.

We carry out aperture photometry with the PHOT task in the IRAF DIGIPHOT package. Since KBOs are so faint, the uncertainties in their magnitudes are dominated by sky noise. Under such conditions, it is common in stellar photometry to use a small aperture for the instrumental magnitude measurements, in order to minimize the sky noise, and to make an “aperture correction” to the “total magnitude” using observations in a small and large aperture on a brighter star, a point spread function (PSF) star, in the same image as the KBO. For each image, our small and large apertures are 3 pixels and 15 pixels in radius. The typical size of the aperture correction is ~0.5 magnitudes. Our sky annulus has radii of 15 and 25 pixels. We take the sky brightness in each image as the peak of a gaussian fit to the histogram of pixel values in the annulus. If necessary, we first clean the annulus of any faint stars or galaxies that might bias the sky measurement by replacing the faint objects with patches of nearby sky.

The brightness of the standard stars and the large aperture of the Keck telescope require us to observe standard stars in “focus mode.” In focus mode, peculiar to the Keck telescopes, the individual mirrors are intentionally misaligned slightly so that we simultaneously obtain 36 separate images of each standard star on the CCD, i.e., one image for each of the 36 mirror segments in the primary mirror. Because sky noise is small in our standard star measurements, we use a single large aperture with a radius of 50 pixels to catch all the light from the 36 images and a sky annulus with radii of 50 and 60 pixels.

We put our KBO colors on the Kron–Cousins photometric system using nightly observations of standard stars (Landolt, 1992). We derive extinction coefficients (magnitudes airmass⁻¹) from observations of seven standard stars in the G163 and PG1633 + 099 fields at small (1.0 < secz < 1.2) and large (1.8 < secz < 2.1) airmass values,

$$k_B = 0.19 - 0.01(B-V) \quad (1)$$

$$k_V = 0.11 \quad (2)$$

$$k_R = 0.08. \quad (3)$$

Using the coefficients, we then correct the standard star and KBO instrumental magnitudes (b , v , and r) to their values above the atmosphere of the Earth (b_o , v_o , and r_o). Next, we use standard star measurements with small airmass values, 1.0 < secz < 1.2, to derive transformation equations

Table 1
Number of standard star exposures

Field	Stars	B	V	R
G163	50,51	14	6	7
PG1633 + 099	PG,A,B,C,D	13	6	7
MARK	A1,A2,A3	4	2	2

between instrumental colors and Kron–Cousins colors. In Table 1, we present a summary of the 208 standard star measurements with $1.0 < \text{secz} < 1.2$; i.e., we list the number of exposures per field and filter. In Fig. 1a, each open circle represents the Kron–Cousins B–V color (Landolt 1992) and our measurement of the average instrumental color of a standard star for a night, $b_o - v_o$. The nightly $b_o - v_o$ measurements of each standard star exhibit a scatter of ~ 0.005 magnitudes about the mean. For example, we find PG1633 + 099 B has average $b_o - v_o$ values of 1.313, 1.315, and 1.308 on nights 1, 2, and 3. In Fig. 1b, we present the values for V–R and $v_o - r_o$. The best fit to the open circles in Figs. 1a and 1b are given by

$$(B-V) = 1.023(b_o - v_o) - 0.264 \quad (4)$$

$$(V-R) = 1.094(v_o - r_o) + 0.030. \quad (5)$$

When we input our standard star measurements of $b_o - v_o$ and $v_o - r_o$ into the transformation equations and then compare the resulting B–V and V–R values with the values

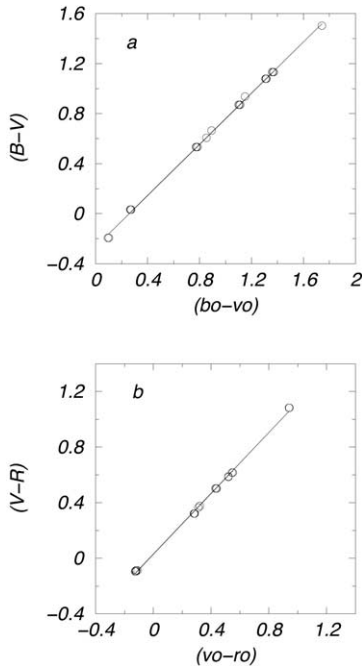


Fig. 1. (B–V) and (V–R) transformation equations for LRIS and the 10-m Keck I telescope. (a) Each open circle represents the Landolt (B–V) value and the average $(b_o - v_o)$ value of a standard star for a night. The solid line represents the best straight line fit to the open circles, the (B–V) transformation equation. (b) Same as (a), but for (V–R).

Table 2
Number of Keck KBO exposures—May 2001

KBO	B ^a	V ^b	R ^b
2000 KK4	4	2	2
2000 FS53	8	4	4
1999 HV11	6	3	3
1999 HS11	6	3	3
1998 KS65	8	4	4
1998 KR65	6	3	3
1998 HM151	9	5	5
1998 HJ151	8	4	4
1998 FS144	6	3	3
1997 CV29	6	3	3
1994 JQ1	4	2	2
1993 FW	5	2	3

^a 520-s exposures in B.

^b 600-s exposures in V and R.

in Landolt (1992), we find residuals ≤ 0.01 magnitudes. For example, when we insert the average $b_o - v_o$ value for PG1633+099 B on night one, 1.313, into Eq. (4), we obtain $B-V = 1.079$, whereas Landolt gives $B-V = 1.081$.

In Table 2, we present a summary of our May 2001 KBO measurements on the Keck by object and filter. Notice that for each object the sum of the number of V and R exposures equals the number of B exposures. This pattern is due to our ability to collect either B and V images or B and R images simultaneously. We see from Table 2 that our colors of 12 KBOs come from 153 Keck images. The airmass values of our KBO observations span the range $1.1 < \text{secz} < 1.5$.

III. Colors and orbital elements

In Table 3, we present our latest observations. Measurements for 12 objects come from the Keck I 10-m telescope, and measurements for 6 objects come from the University of Arizona 2.3-m telescope and the Vatican Observatory 1.8-m telescope. A description of the 2.3-m and 1.8-m telescopes and their CCD cameras is in the literature (Tegler and Romanishin, 1997; Romanishin et al., 2001). From a dozen or more images taken on the 2.3-m and 1.8-m telescopes in each of the B, V, and R filters per object, we find that 20000 Varuna, 1999 UG5, 1999 TD10, and 1998 SG35 exhibit brightness variations (lightcurves). A future paper will describe the lightcurves of these four objects. In order to minimize the effect of the lightcurve on the colors, we obtain our images in a R–V–B–B–V–R sequence. The colors of the six objects in Table 3 taken on the 2.3-m and 1.8-m telescopes are the average of a dozen or more measurements of B–V and V–R. The V magnitudes for the four objects with lightcurves are our best estimates of the median V magnitudes, i.e. $(V_{\max} + V_{\min})/2$.

In Fig. 2a, we combine the 18 new color measurements in Table 3 with our previous 32 measurements (Tegler and

Table 3
Optical colors, primarily from May 2001 at the Keck I telescope

Object	Class	q^c	V	$\frac{\sigma}{\sqrt{n}}$	B-V	$\frac{\sigma}{\sqrt{n}}$	V-R	$\frac{\sigma}{\sqrt{n}}$	UT
20000 Varuna ^a	Clas	40.87	20.45	0.05	0.96	0.08	0.56	0.02	2001 Apr 17,18
2000 EB173 ^a	Plu	28.55	19.78	0.04	1.00	0.06	0.60	0.03	2001 Apr 17,18
2000 KK4	Plu	36.79	22.96	0.02	0.91	0.04	0.64	0.03	2001 May 22
2000 FS53	Clas	41.44	24.21	0.06	1.06	0.04	0.71	0.02	2001 May 23
1999 UG5 ^{a,b}	Cen	7.47	19.23	0.08	1.08	0.05	0.67	0.01	1999 Nov 8,11,12
1999 TD10 ^{a,b}	Cen	12.30	20.20	0.05	0.77	0.02	0.47	0.01	1999 Nov 8,11,12
1999 HV11	Clas	40.79	23.95	0.03	1.11	0.06	0.59	0.02	2001 May 21
1999 HS11	Clas	43.10	23.38	0.03	1.14	0.03	0.72	0.02	2001 May 22
1998 SG35 ^{a,b}	Cen	5.83	21.53	0.02	0.73	0.02	0.48	0.01	1999 Nov 8,9,11
1998 KS65	Clas	42.28	24.05	0.02	1.09	0.04	0.64	0.02	2001 May 21
1998 KR65	Clas	42.43	23.72	0.03	1.13	0.02	0.67	0.02	2001 May 23
1998 HM151	Clas	43.48	24.36	0.05	0.93	0.09	0.62	0.05	2001 May 22
1998 HJ151	Clas	41.05	23.91	0.02	1.11	0.03	0.71	0.03	2001 May 21
1998 FS144	Clas	40.45	23.55	0.02	0.96	0.02	0.57	0.02	2001 May 21
1997 CV29	Clas	40.25	23.86	0.01	1.21	0.01	0.65	0.02	2001 May 22
1995 SM55 ^a	Clas	37.48	20.55	0.01	0.65	0.01	0.39	0.01	1999 Nov 11,12
1994 JQ1	Clas	41.86	23.51	0.03	1.12	0.02	0.63	0.02	2001 May 21
1993 FW	Clas	41.66	23.43	0.01	1.03	0.05	0.63	0.01	2001 May 23

^a Vatican Observatory 1.8-m telescope.

^b University of Arizona 2.3-m telescope.

^c Perihelion distance in AU.

Romanishin, 1998; Tegler and Romanishin, 2000) for a sample size of 50 objects. In Fig. 2b, we plot the colors of 57 objects obtained by the other research groups, i.e., the com-

parison sample (Barucci et al., 1999; Barucci et al., 2000; Boehnhardt et al., 2001; Delsanti et al., 2001; Jewitt and Luu, 2001; Doressoundiram et al., 2002), on axes identical

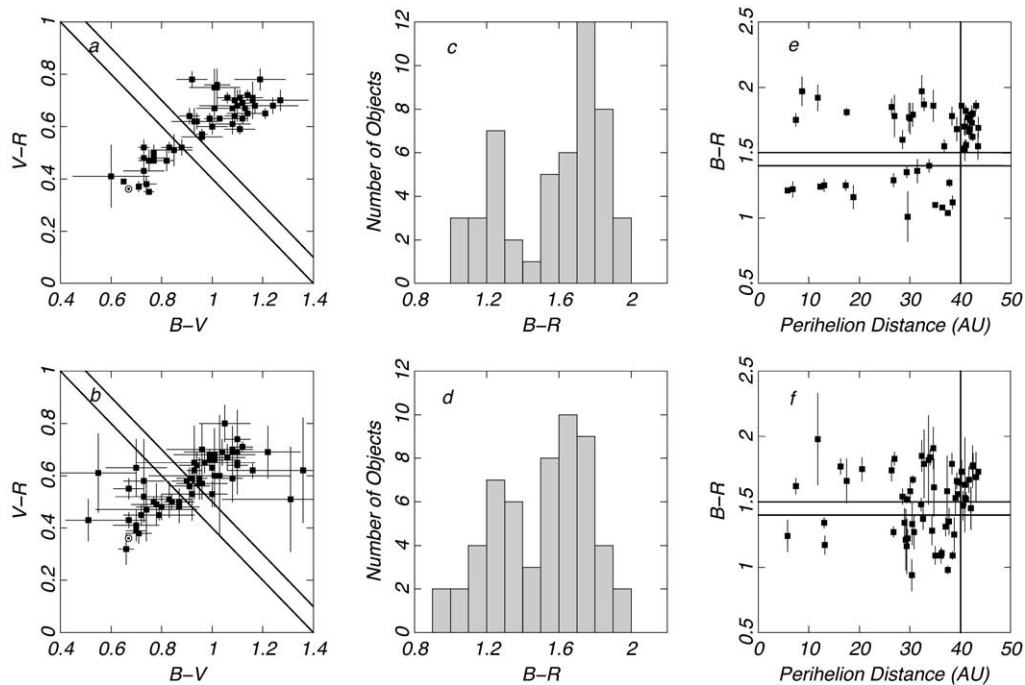


Fig. 2. Observations of Kuiper belt object surface colors by our group, top row, and other groups, bottom row. (a,b) Color-color diagrams of the 50 objects in our survey and 57 objects in the literature. The color of the Sun is represented by the standard solar symbol at $B-V = 0.67$ and $V-R = 0.36$. The reddest objects are toward the upper right-hand corner of each figure. The points of both figures occupy the same diagonal region and exhibit a minimum in their surface density near $B-V = 0.87$, $V-R = 0.56$. (c,d) $B-R$ histograms of the data in the color-color diagrams that come from the sums of $B-V$ and $V-R$ values. The reddest objects are in bins with the largest values of $B-R$. There is a definite double peaked distribution of colors in both figures. (e,f) Plots of $B-R$ color against perihelion distance for the objects in our survey and in the literature. In both figures, objects with $q < 40$ AU exhibit red ($B-R > 1.5$) or gray ($B-R < 1.4$) colors and objects with $q > 40$ exhibit only red ($B-R > 1.5$) colors.

to Fig. 2a. We do not include the data of Luu and Jewitt (1996) and Jewitt and Luu (1998) in Fig. 2b. Jewitt and Luu (2001) remeasured eight objects from their earlier two papers. Seven of the eight B–R remeasurements are ~ 0.3 magnitudes redder than the original values. In the case of the bright ($V = 20.91$) object 1996 TL66, Jewitt and Luu report a B–R color 0.39 magnitudes redder than their original value. The seven remeasured B–R values agree at the 0.10-magnitude level or better with all the other values in the literature, including our values. We believe there is a systematic problem with the colors in the first two papers of Jewitt and Luu. The points in Fig. 2b represent all the moderate- to large-aperture telescope measurements of Kuiper belt object BVR colors in the literature with the exception of the first two papers of Jewitt and Luu.

In Table 4 where we give only the B–R colors of our sample and the comparison sample, we see almost 40% (i.e., 21) of the 57 objects have been independently measured by more than one of the other groups, and for each of these objects we simply compute the average B–V, V–R, and B–R colors.

In Table 4 we see that almost 50% (i.e., 27) of the 57 objects in the comparison sample are in our sample. For 18 of the 27 objects in both samples, we find the average B–R color of the comparison sample (column 7) and the B–R color in our survey (column 8) differ by ≤ 0.1 magnitudes, i.e., good agreement between the samples.

There are remarkable similarities between Figs. 2a and 2b. In particular, the points of both figures occupy the same diagonal region and exhibit a minimum in their surface density at about $B-V = 0.87$ and $V-R = 0.56$. This minimum separates the red and gray populations in the figures. The color of the Sun is represented by the standard solar symbol at $B-V = 0.67$ and $V-R = 0.36$, and the reddest objects are toward the upper right-hand corner of each figure.

The most striking difference between Figs. 2a and 2b is that our data points exhibit much smaller error bars than the data points in the comparison sample. Our average B–V uncertainty is 0.05 magnitude and the comparison sample average B–V uncertainty is 0.10 magnitude. Our average V–R uncertainty is 0.04 magnitude and the comparison sample average V–R uncertainty is 0.08 magnitude. Our average uncertainty is half of the comparison sample average uncertainty. Since the data points in both figures primarily come from measurements made with 8-m (VLT) and 10-m (Keck) class telescopes, it appears our smaller error bars are the result of our longer exposure times per object. For example, we obtain B, V, and R images of 12 objects in Table 3 during three full photometric nights on the Keck I telescope and LRIS. We were able to greatly increase our observational efficiency by using a dichroic element and two CCDs making it possible for us to obtain simultaneous B and R or B and V images. Nine of our 12 objects had exposure times of at least 3120 s in B, 1800 s in V, and 1800 s in R. One object, 1998 HM151, had a 4680-s expo-

sure time in B and a 3000-s exposure time in each of V and R. Jewitt and Luu (2001) obtained B, V, R, and I images of 25 objects during only two nights on the Keck II telescope and LRIS. At the time of their observations, Jewitt and Luu were not able to gather two images simultaneously. Their exposure times range from only 200 to 500 s per object per filter.

The existence of two color populations is quite striking in a B–R histogram. We obtain the B–R color for each object in Figs. 2a and 2b from the sum of their B–V and V–R colors. We present the B–R histogram of our data and the comparison sample in Figs. 2c and 2d, respectively. For reference, the Sun has a B–R color of 1.03. We see striking similarities between the two histograms. Specifically, both histograms exhibit a peak in the $1.2 < B-R < 1.3$ bin. Our histogram has a second peak in the $1.7 < B-R < 1.8$ bin and the comparison sample histogram has a second peak in the $1.6 < B-R < 1.7$ bin. In addition, both histograms exhibit a paucity of objects in the $1.4 < B-R < 1.5$ bin. An object with $1.4 < B-R < 1.5$ resides between the diagonal lines in Figs. 2a and 2b.

Perhaps the most striking case for two color populations is seen in a plot of B–R color against perihelion distance, q , for our survey, Fig. 2e, and the comparison sample, Fig. 2f. The overwhelming majority of objects with $q < 40$ AU in both data sets exhibit $B-R < 1.4$ or $B-R > 1.5$. Only one object in each of Figs. 2e and 2f has $q < 40$ AU and $1.4 < B-R < 1.5$. In addition, we find 20 out of 20 objects with $q > 40$ AU in our survey exhibit extremely red surface colors, $B-R > 1.5$. Twelve of the 20 objects are new measurements in Table 3. Both our survey and the comparison survey find no objects with $q > 40$ AU and $B-R < 1.4$. Both data sets appear consistent with red and gray populations for $q < 40$ AU and only a red population for $q > 40$ AU, a confirmation of our earlier work (Tegler and Romanishin, 2000).

There are a sufficient number of KBOs in the data sets to look for patterns within the plutino and classical KBO dynamical classes. Plutinos are on stable Pluto-like orbits in a 2:3 resonance with Neptune and fall near the dashed vertical line at ~ 39.4 AU in Figs. 3a (our data set) and 3b (the comparison data set). Classical KBOs are on low-eccentricity orbits and fall near a ~ 43 AU in the figures. KBOs with $q \geq 40$ AU fall on and below the curve toward the lower right-hand corners of Figs. 3a and 3b. In both figures, we represent red KBOs ($B-R > 1.5$) with plus symbols and gray KBOs ($B-R < 1.5$) with circles. In our data set, 20 of 20 classical KBOs on low-eccentricity orbits and $q > 40$ AU exhibit extremely red colors. In the comparison data set, 10 of 12 classical KBOs on low-eccentricity orbits and $q > 40$ AU exhibit extremely red colors. The two exceptions in the comparison data set, 1998 FS144 and 1999 HR11, have B–R colors of 1.47 ± 0.11 and 1.45 ± 0.16 , putting them just below our $B-R > 1.5$ cutoff for the red group. Classical KBOs on low-eccentricity orbits exhibit only extremely red surface colors, a confirmation of

Table 4
B–R measurements of 57 objects in the literature

Object	1	2	3	4	5	Literature avg	Our survey
2000 QC243		1.17				1.17 ± 0.07	
2000 PE30					1.09	1.09 ± 0.06	
2000 OK67		1.25				1.25 ± 0.13	
2000 EB173	1.58				1.49	1.54 ± 0.05	1.60 ± 0.07
1999 UG5		1.62				1.62 ± 0.06	1.75 ± 0.05
1999 TC36		1.72		1.66	1.64	1.67 ± 0.02	
1999 RY215					1.28	1.28 ± 0.11	
1999 OX3					1.66	1.66 ± 0.17	1.81 ± 0.03
1999 KR16	1.84					1.84 ± 0.06	
1999 HS11					1.69	1.69 ± 0.19	1.86 ± 0.04
1999 HR11					1.45	1.45 ± 0.16	
1999 HB12					1.37	1.37 ± 0.08	
1999 DE9	1.51	1.44				1.48 ± 0.04	
1999 CD158		1.35				1.35 ± 0.10	
1999 CC158		1.53				1.53 ± 0.12	
1998 XY95				1.58		1.58 ± 0.27	
1998 WV31		1.34				1.34 ± 0.11	
1998 WH24		1.59	1.49	1.47		1.52 ± 0.04	1.56 ± 0.04
1998 VG44				1.54	1.50	1.52 ± 0.02	
1998 UR43		1.27				1.27 ± 0.13	
1998 TF35		1.81		1.73		1.77 ± 0.04	
1998 SN165	1.11	1.06			1.15	1.11 ± 0.03	
1998 SM165		1.58				1.58 ± 0.09	1.76 ± 0.12
1998 SG35		1.15			1.32	1.24 ± 0.09	1.21 ± 0.02
1998 KG62					1.53	1.53 ± 0.08	
1998 HK151					0.94	0.94 ± 0.12	
1998 FS144			1.47			1.47 ± 0.11	1.53 ± 0.03
1998 BU48		1.75				1.75 ± 0.09	
1997 QJ4	1.33					1.33 ± 0.16	
1997 QH4	1.70	1.62				1.66 ± 0.04	1.68 ± 0.09
1997 CU29	1.71		1.93		1.71	1.78 ± 0.07	
1997 CU26	1.34					1.34 ± 0.04	1.25 ± 0.05
1997 CS29	1.77		1.71	1.71		1.73 ± 0.02	1.69 ± 0.08
1997 CR29	1.36				1.26	1.31 ± 0.05	
1997 CQ29	1.63		1.67			1.65 ± 0.02	
1996 TS66	1.79					1.79 ± 0.08	1.78 ± 0.07
1996 TQ66	1.91					1.91 ± 0.16	1.86 ± 0.12
1996 TP66	1.82		1.79	1.61		1.74 ± 0.07	1.85 ± 0.06
1996 TO66	1.12		1.12	1.04		1.09 ± 0.03	1.12 ± 0.05
1996 TL66	1.10		1.18	0.98		1.09 ± 0.06	1.10 ± 0.02
1996 TK66	1.77					1.77 ± 0.16	1.62 ± 0.03
1996 SZ4	1.16					1.16 ± 0.21	1.35 ± 0.04
1996 RR20	1.79					1.79 ± 0.26	1.87 ± 0.05
1996 RQ20	1.54	1.56		1.57		1.56 ± 0.01	
1995 WY2	1.63					1.63 ± 0.36	
1995 TL8		1.73				1.73 ± 0.09	
1995 SM55		1.00		0.96		0.98 ± 0.02	1.04 ± 0.01
1995 QY9			1.21			1.21 ± 0.23	
1995 HM5			1.22			1.22 ± 0.07	1.01 ± 0.19
1995 DA2	1.82					1.82 ± 0.34	
1994 TB	1.90	1.76	1.84			1.83 ± 0.04	1.78 ± 0.16
1994 TA	1.98					1.98 ± 0.35	1.92 ± 0.10
1994 JR1			1.61			1.61 ± 0.22	
1993 SC	1.85					1.85 ± 0.12	1.97 ± 0.12
1993 SB	1.29	1.23				1.26 ± 0.03	1.29 ± 0.05
1993 FW			1.67			1.67 ± 0.10	1.66 ± 0.05
1992 QB1	1.65			1.60		1.63 ± 0.03	1.70 ± 0.07

Notes. (1) Jewitt and Luu 2001; (2) Delsanti et al., 2001; (3) Barucci et al., 1999, 2000; (4) Boehnhardt et al., 2001; (5) Doressoundiram et al., 2001.

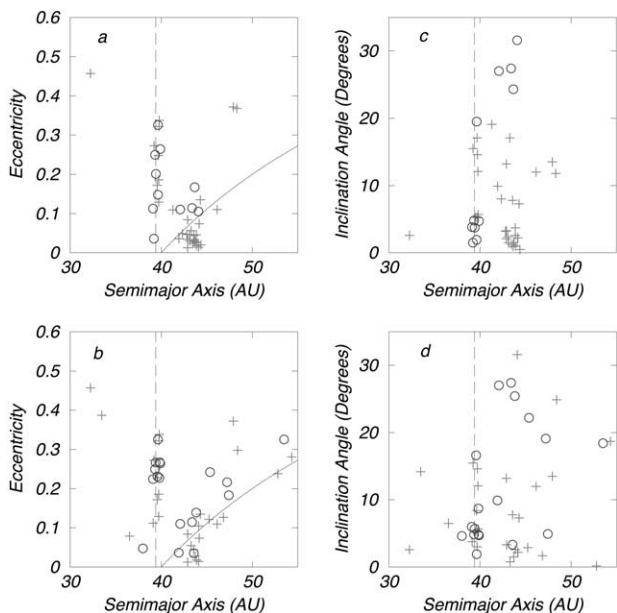


Fig. 3. Colors and dynamical properties for our data set, top row, and the comparison data set, bottom row. Pluses represent red ($B-R > 1.5$) surface colors and circles represent gray ($B-R < 1.5$) surface colors. (a,b) Classical KBOs (~ 43 AU) on low-eccentricity orbits exhibit only extremely red surface colors. (c,d) Classical KBOs on low-inclination angle orbits exhibit only extremely red surface colors.

our earlier work (Tegler and Romanishin, 2000). Plutinos do not exhibit any correlation between color and eccentricity.

In addition to a correlation between color and eccentricity, classical KBO exhibit a correlation between color and inclination angle. In Fig. 3c (our data set), we see that classical KBOs on low-inclination orbits ($i < 20^\circ$) exhibit extremely red surface colors. In addition, four of four classical KBOs with $i > 20^\circ$ exhibit gray surface colors. The comparison data set (Fig. 3d), has a similar correlation. We were the first to point out the correlation between color and inclination angle for classical KBOs (Tegler and Romanishin, 2000). Recently, Brown and Trujillo (2002) confirm the inclination pattern. Plutinos do not exhibit any correlation between inclination angle and color.

IV. Monte Carlo simulations

Are the data sets consistent with two color populations in a statistical sense? Do the data sets rule out a continuum of colors? In order to answer these questions, we have run Monte Carlo simulations, assuming two underlying distributions of “true colors,” i.e., colors we would measure if we had no observational uncertainties. The first distribution, the continuum or continuous distribution, consists of a continuous line of colors from $B-V = 0.67$, $V-R = 0.40$ to $B-V = 1.15$, $V-R = 0.70$ on a color-color diagram. The second distribution, the bimodal distribution, consists of the same continuous line of “true colors” as the continuous distribu-

tion, but with the central one-third of the line missing. Specifically, the bimodal distribution consists of objects populating a gray line from $B-V = 0.67$, $V-R = 0.40$ to $B-V = 0.83$, $V-R = 0.50$, and objects populating a red line from $B-V = 0.99$, $V-R = 0.60$ to $B-V = 1.15$, $V-R = 0.70$. We assume a uniform probability of obtaining any given color within the red line, the gray line, and the continuum line. The number of object in each line is specified. For a given run, we generate 50 “true colors” to simulate our data in Fig. 2a, or 57 “true colors” to simulate the comparison data in Fig. 2b, using a random number generator to pick colors along each line segment. For the bimodal model, we have about 50% more red than blue objects to match the observed distribution. Once we generate the “true colors,” we simulate the observational uncertainties with a Gaussian-weighted random number generator. That is, we assume the actual measurement result will fall about the neighborhood of the “true color” with a probability given by a Gaussian function.

In Fig. 4, we present color-color plots for three typical runs of 57 objects and a bimodal “true color” distribution (the gray filled circles). Each run has different widths (i.e., σ_{B-V} and σ_{V-R}) for the Gaussian uncertainty functions. Fig. 4a has observational uncertainties that match ours, while 4b has uncertainties equal to the average in the comparison sample. As the width increases, it is more difficult to recognize the two “true color” populations. As seen in Fig. 4c, once the uncertainties in $B-V$ and $V-R$ reach 0.12 and 0.08, the two color populations are almost impossible to see in a color-color diagram. In Fig. 4, we see that large uncertainties make the two color populations look like a continuum of colors.

How can we best test the validity of the continuous and bimodal model color distributions? $B-R$ histograms of a large number of objects chosen from the two models using a wide range of assumed uncertainties shows the expected result—the continuous color distribution results in observed histograms flat across the central region, while the bimodal color distribution results in a dip between the putative gray and red color groups. The dip is centered in the $1.4 < B-R < 1.5$ color bin, so looking at the number of objects in this bin provides the most sensitive discrimination between the two models.

In order to quantify whether the data support two populations and/or a continuum of colors, we made 1000 Monte Carlo runs and then found the number of times that 0, 1, 2, 3, 4, . . . objects fell into the $1.4 < B-R < 1.5$ bin, i.e., the central bin, which corresponds to the proposed minimum in surface density of points on the color-color diagrams. In Fig. 5a, we present our results for 1000 runs with a bimodal color distribution, 50 objects, and σ_{B-V} and σ_{V-R} equal to the average of our error bars in Fig. 2a. In this case, we find 333 out of 1000 runs yield one object in the central bin. In Fig. 5b, we present our results for 1000 runs with a bimodal color distribution, 57 objects, and σ_{B-V} and σ_{V-R} equal to the average of the comparison sample error bars in Fig. 2b.

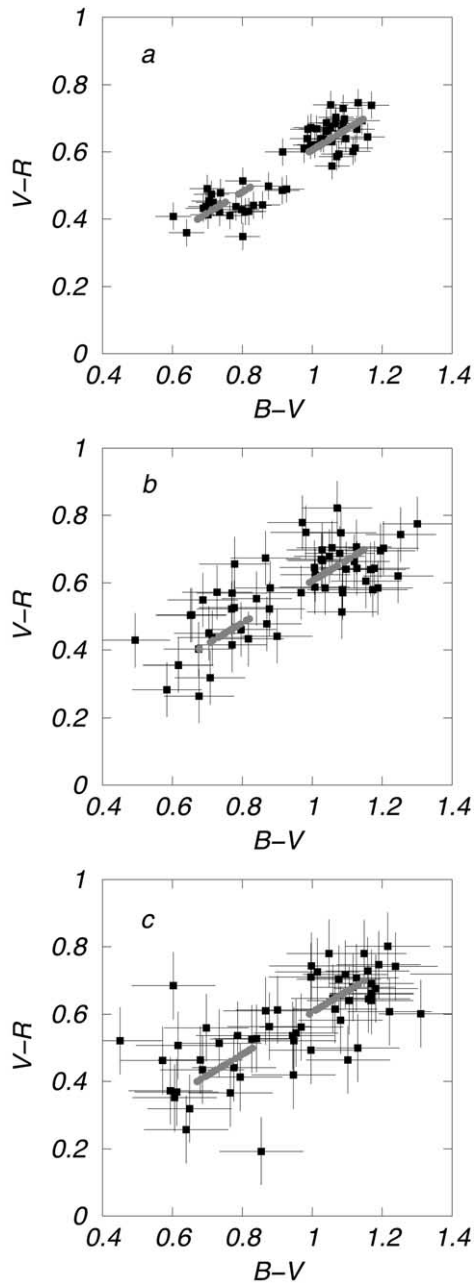


Fig. 4. A typical Monte Carlo simulation of Kuiper belt object color observations, assuming that the “true colors” of 57 objects (filled gray circles) result from the assumption of a bimodal color distribution—i.e., a gray population between $B-V = 0.67$, $V-R = 0.40$ and $B-V = 0.83$, $V-R = 0.50$, and a red population between $B-V = 0.99$, $V-R = 0.60$ and $B-V = 1.15$, $V-R = 0.70$. The effect of observational uncertainties is included by tweaking the “true colors” with a Gaussian-weighted random number generator (filled black squares). (a) Gaussian widths of $\sigma_{B-V} = 0.05$ and $\sigma_{V-R} = 0.04$. (b) $\sigma_{B-V} = 0.10$ and $\sigma_{V-R} = 0.08$. (c) $\sigma_{B-V} = 0.12$ and $\sigma_{V-R} = 0.08$. As the Gaussian widths increase, it becomes difficult to see the two color populations. For large widths the two populations take on the appearance of a continuum of colors.

In this case, we find 212 out of 1000 runs yield three objects in the central bin. In other words, the simulations indicate our observation of one object and the other investigators’

observation of three objects in the central bin will occur often for a bimodal color distribution. Thus, both data sets are consistent with two color populations.

In Fig. 5c, we present our results for 1000 runs with a continuous color distribution, 50 objects, and σ_{B-V} and σ_{V-R} equal to the average of our error bars in Fig. 2a. In this case, we find only two out of 1000 runs yield one object in the central bin. In Fig. 5d, we present our results for 1000 runs with a continuous color distribution, 57 objects, and σ_{B-V} and σ_{V-R} equal to the average of the comparison sample error bars in Fig. 2b. In this case, we find 36 out of 1000 runs yield three objects in the central bin. In other words, the simulations indicate our observation of one object in the central bin will rarely occur for a continuous color distribution. Our data set rules out a continuum of colors for Kuiper belt objects at the 3σ level. Simulations of the comparison data set and a continuous color distribution indicate three or fewer objects will occur in the central bin 5% of the time; therefore, a continuum color distribution is improbable for the comparison sample. It is important to realize that division of the ordinate values in Fig. 5 by 1000 gives the probabilities of obtaining 0,1,2,3,4, . . . objects in the central bin. We notice that the number of objects we

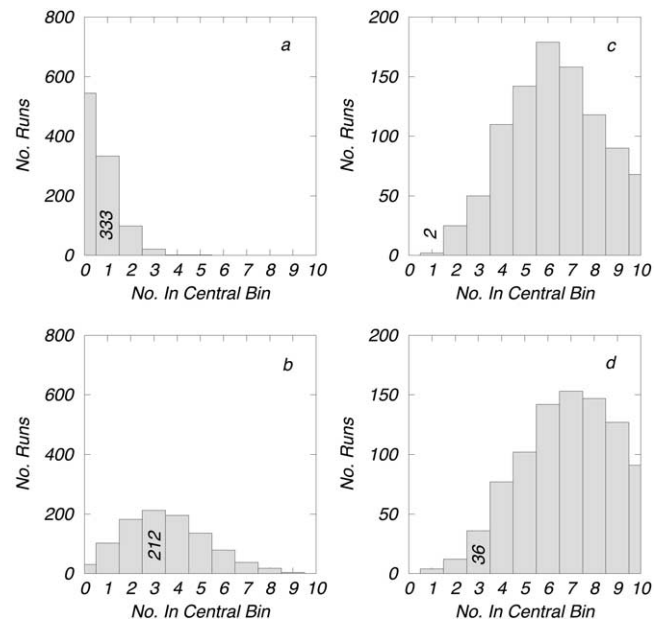


Fig. 5. The number of runs in which 0,1,2,3,4, . . . objects fall into the central bin at $1.4 < B-R < 1.5$ out of a total of 1000 Monte Carlo runs. (a) For a bimodal distribution of “true colors” and a simulation of our observational uncertainties, one object falls in the central bin 333 out of 1000 runs, a frequent event. (b) For a bimodal distribution of “true colors” and a simulation of the comparison sample observational uncertainties, three objects fall in the central bin 212 out of 1000 runs, a frequent event. (c) For a continuous distribution of “true colors” and a simulation of our observational uncertainties, one object falls in the central bin 2 out of 1000 runs, a very rare event. (d) For a continuous distribution of “true colors” and a simulation of the comparison sample observational uncertainties, three objects fall in the central bin 36 out of 1000 runs, an unlikely event. Our data set and the simulations rule out a continuous distribution of “true colors” for Kuiper belt objects.

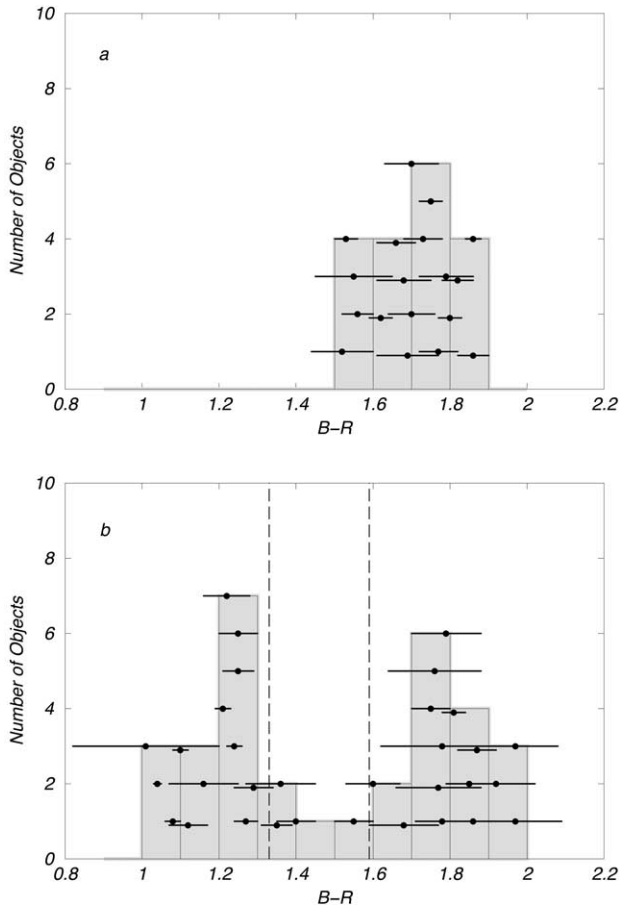


Fig. 6. B–R histogram of the objects in our survey. (a) All 18 objects with $q > 40$ exhibit extremely red surface colors, $B-R > 1.5$. The probability of 18 out of 18 objects exhibiting $B-R > 1.5$ for a continuous distribution of colors is only $(1/2)^{18}$. (b) The 32 objects in our survey with $q < 40$ appear to exhibit a bimodal color distribution. We expect four or fewer measurements in the central bin to occur only 5 out of 1000 times we measure 32 KBOs with a continuous color distribution.

actually observe in the central bin are near the peak probabilities for the bimodal distribution (Figs. 5a and 5b) and out in the wings for the continuous color distribution (Figs. 5c and 5d).

The preceding analysis used all the dynamical classes of objects. As noted in Section III, we and others find that objects with $q > 40$ AU are exclusively red. Although the exact relationship between the $q > 40$ AU and $q < 40$ AU populations are unclear, the $q > 40$ AU population may be distinct from the $q < 40$ AU population. Because the $q > 40$ AU population is exclusively red, it may be somehow biasing the total sample in a way to mimic a bimodal population. Thus, we have carried out separate Monte Carlo tests of the bimodal and continuous color distributions using only the $q < 40$ AU observed samples.

In Fig. 6, we present B–R histograms of our observations, split into $q > 40$ AU and $q < 40$ AU samples. In Fig. 6a, we see that 18 out of 18 objects with $q > 40$ AU are redder than the midpoint of our bimodal distribution. The

chance of this happening, if the objects are really chosen from a continuous distribution, is $(1/2)^{18} = 4 \times 10^{-6}$. In Fig. 6b, we see the B–R colors of our $q < 40$ AU group exhibit a strong bimodal appearance. In Fig. 7, we present the analogous B–R histograms for the comparison sample. Overall, Figs. 6 and 7 are strikingly similar. The $q < 40$ AU samples (32 objects for our sample and 45 objects for the comparison sample) are split remarkably evenly around the midpoint ($B-R = 1.46$) of the extremes of our model color distributions.

We redid the Monte Carlo calculations for the $q < 40$ AU samples. The results of these calculations are shown in Fig. 8. In Fig. 8a and 8b, we present the number of objects in the central bin ($1.4 < B-R < 1.5$) for the bimodal distribution using sample sizes and observational uncertainties appropriate for our observations and the comparison sample observations. In Figs. 6 and 7, we see that both observational samples only have one object in the central bin. We find 278 out of 1000 runs yield one object in the central bin for the simulation of our data and 178 out of 1000 runs yield one object in the central bin for the simulation of the comparison sample data. Thus, both samples are consistent with the bimodal color distribution.

We also tested the continuous color distribution for the q

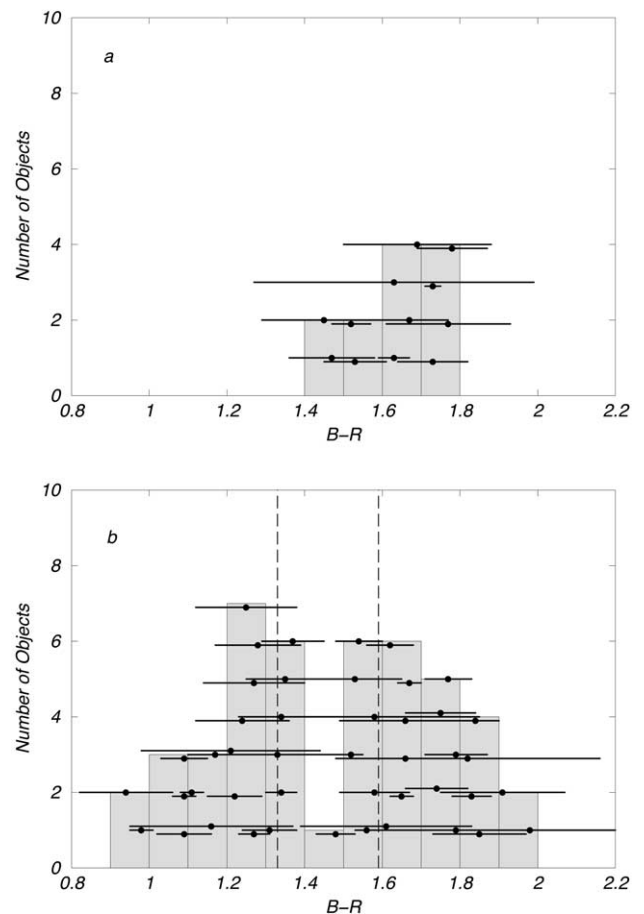


Fig. 7. Same as Fig. 6, but for comparison sample.

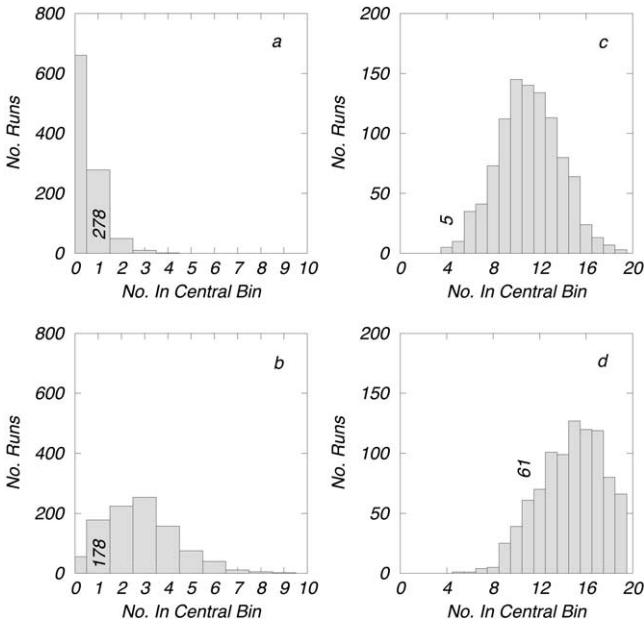


Fig. 8. Same as Fig. 5, but for the $q < 40$ AU samples only. (a) For a bimodal distribution of “true colors” and a simulation of our observational uncertainties, one object falls in the central bin ($1.4 < B-R < 1.5$) 278 out of 1000 runs, a frequent event. (b) For a bimodal distribution of “true colors” and a simulation of the comparison sample observational uncertainties, one object falls in the central bin ($1.4 < B-R < 1.5$) 178 out of 1000 runs, a frequent event. (c) For a continuous distribution of “true colors” and a simulation of our observational uncertainties, four objects fall in the wide central bin ($1.33 < B-R < 1.59$) five out of 1000 runs. (d) For a continuous distribution of “true colors” and a simulation of the comparison sample uncertainties, 11 objects fall in the wide central bin ($1.33 < B-R < 1.59$) 61 out of 1000 runs. Eleven or fewer objects fall in the wide central bin for 14% of the runs.

< 40 AU sample using the Monte Carlo technique. However, because of the significantly smaller number of objects in the $q < 40$ AU sample than the full sample, the use of 0.1 $B-R$ bins results in too few objects per bin to produce a conclusive test of the continuous color distribution model. As the continuous color model has a uniform distribution of colors, with no sharp changes of number vs color in the assumed distribution, use of a wider bins is acceptable, and greatly increases the possibility of making a conclusive test of the continuous color distribution for this smaller population. Therefore, to test the continuous color distribution, we compared the number of objects observed and predicted by the Monte Carlo code in a wide central bin ($1.33 < B-R < 1.59$). This bin was not chosen arbitrarily, of course—it is the complete extent of the gap in the colors for our bimodal distribution.

The results of this test of the continuous color distribution for the $q < 40$ AU samples are shown in Fig. 8c and 8d. In our observed $q < 40$ AU sample, we find four out of 32 objects in the wide central bin with observed colors $1.33 < B-R < 1.59$. The Monte Carlo calculations indicate that four objects occur in the wide central bin only five out of 1000 times for a continuous color distribution, and four or

fewer objects occur about 0.5% of the time. For the comparison sample, there are 11 out of 45 objects with $1.33 < B-R < 1.59$. The models predict 11 objects occur in the wide central bin 61 out of 1000 times for a continuous color distribution, and 11 or fewer objects occur about 14% of the time. Thus, the comparison sample cannot rule out the continuous distribution, although we see in Fig. 8d that the observed number of objects is noticeably below the peak of the number expected in the central bin for a continuous color distribution.

We summarize the proceeding discussion as follows: Using both our sample and the comparison sample, it is clear that objects with $q > 40$ AU are exclusively red. Both the complete and $q < 40$ AU comparison samples are consistent with either the continuous or bimodal color distributions. Both our complete and $q < 40$ AU samples are consistent with the bimodal distribution, but rule out the continuous distribution at $\sim 3\sigma$ level. Of course, finding that all samples are consistent with the bimodal distribution (and that the comparison samples are consistent with the continuous distribution) does not prove that either the bimodal or continuous distributions match reality. *However, it is important to realize our observations do rule out the continuous color distribution.* The fact that the comparison samples are consistent with the continuous distribution does not negate our conclusion that the continuous distribution is ruled out, but shows that our smaller uncertainties allow us to draw a conclusive statement about the continuous color distribution that the comparison sample, with its larger uncertainties, is not able to draw.

V. Conclusions

We can draw three important conclusions from the above analysis of 80 KBOs and Centaurs. First, color measurements of 27 KBOs and Centaurs common to our sample and the comparison sample are consistent. Second, it appears that the debate over a continuum of colors vs two color populations is the result of measurement uncertainties. Specifically, we believe that other investigators would see two color groups if their measurements had smaller uncertainties. Finally, classical KBOs in our sample and the comparison sample with perihelion distances beyond 40 exhibit extremely red surface colors.

Our conclusions are difficult to reconcile with known processes in the outer Solar System. For example, the collisional-graying and radiation-reddening mechanism predicts color variations with rotational phase over the surface of an individual KBO. Repeated measurements of individual KBOs at random rotational phases indicate the surface colors of individual KBOs are quite homogeneous. There is no evidence of gray craters on ancient red crusts. Furthermore, the collisional-graying and radiation-reddening mechanism predicts grayer surfaces for objects with large eccentricities and inclination angles. Such a correlation does

appear among the classical KBOs; however, the plutinos exhibit no such correlation. Finally, the collisional-graying and radiation-reddening mechanism predicts a continuum of colors not two groups.

At the present time, we favor neither intrinsic compositional differences among KBOs at the time of their formation nor subsequent evolutionary processes to explain the colors of KBOs. Further observational, theoretical, and laboratory work is necessary to better understand KBO colors.

Acknowledgments

We thank the NASA Planetary Astronomy program for financial support of this research and the NASA-Keck, Steward Observatory, and Vatican Observatory Telescope Allocation Committees for consistent allocation of telescope time.

References

- Barucci, M.A., Doressoundiram, A., Tholen, D., Fulchignoni, M., Lazzarin, M., 1999. Spectrophotometric observations of Edgeworth–Kuiper belt objects. *Icarus* 142, 476–481.
- Barucci, M.A., Romon, J., Doressoundiram, A., Tholen, D.J., 2000. Compositional surface diversity in the trans-Neptunian objects. *Astron. J.* 120, 496–500.
- Boehnhardt, H., Tozzi, G.P., Birkle, K., Hainaut, O., Sekiguchi, T., Vair, M., Watanabe, J., Rupprecht, G., the FORS Instrument Team, 2001. *Astron. Astrophys.* 378, 653–667.
- Delsanti, A.C., Boehnhardt, H., Barrera, L., Meech, K.J., Sekiguchi, T., Hainaut, O.R., 2001. BVRI photometry of 27 Kuiper-belt objects with ESO/Very Large Telescope. *Astron. Astrophys.* 380, 347–358.
- Doressoundiram, A., Barucci, M.A., Romon, J., Veillet, C., 2001. Multicolor photometry of trans-neptunian objects. *Icarus* 154, in press.
- Jewitt, D., Luu, J., 1998. Optical–infrared spectral diversity in the Kuiper belt. *Astron. J.* 115, 1667–1670.
- Jewitt, D.C., Luu, J.X., 2001. Colors and spectra of Kuiper belt objects. *Astron. J.* 122, 2099–2114.
- Landolt, A.U., 1992. UBVRI photometric standard stars in the magnitude range $11.5 < V < 16.0$ around the celestial equator. *Astron. J.* 104, 340–491.
- Luu, J., Jewitt, D., 1996. Color diversity among the Centaurs and Kuiper belt objects. *Astron. J.* 112, 2310–2318.
- Oke, J.B., et al., 1995. The Keck low-resolution imaging spectrometer. *Pub. Astron. Soc. Pac.* 107, 375–385.
- Reif, F., 1965. *Fundamentals of Statistical and Thermal Physics*. McGraw–Hill, New York.
- Romanishin, W., Tegler, S.C., Rettig, T.W., Consolmagno, G., Botthof, B., 2001. 1998 SM165: a large Kuiper-belt object with an irregular shape. *Proc. Nat. Acad. Sci.* 98, 11863–11866.
- Taylor, J.R., 1982. *An Introduction to Error Analysis*. University Science Books, Mill Valley.
- Tegler, S.C., Romanishin, W., 1998. Two distinct populations of Kuiper belt objects. *Nature* 392, 49–51.
- Tegler, S.C., Romanishin, W., 2000. Extremely red Kuiper-belt objects in near-circular orbits beyond 40 AU. *Nature* 407, 979–981.
- Trujillo, C.A., Brown, M.E., 2002. A correlation between inclination and color in the classical Kuiper belt. *Astrophys J.* 566, L125–L128.